Dimmock, A.P.; Nykyri, K.; Karimabadi, Homa; Osmane, A.; Pulkkinen, T.I.

A statistical study into the spatial distribution and dawn-dusk asymmetry of dayside magnetosheath ion temperatures as a function of upstream solar wind conditions

Published in:
Journal of Geophysical Research: Space Physics

DOI:
10.1002/2014JA020734

Published: 01/01/2015

Document Version
Publisher's PDF, also known as Version of record

AGU PUBLICATIONS

JGR

Journal of Geophysical Research: Space Physics

RESEARCH ARTICLE

10.1002/2014JA020734

Key Points:
- The magnetosheath ion temperature is typically 5–10% hotter on the dawn flank
- Magnetosheath temperature asymmetry increases to 15% for fast solar wind speeds
- Magnetosheath ion temperature asymmetry must be driven by kinetic effects

Correspondence to:
A. P. Dimmock,
andrew.dimmock@aalto.fi

Citation:
Dimmock, A. P., K. Nykyri, H. Karimabadi, A. Osmane, and T. I. Pulkkinen (2015), A statistical study into the spatial distribution and dawn-dusk asymmetry of dayside magnetosheath ion temperatures as a function of upstream solar wind conditions, *J. Geophys. Res. Atmos.*, *120*, 2767–2782, doi:10.1002/2014JA020734.

Received 14 OCT 2014
Accepted 23 FEB 2015
Accepted article online 2 MAR 2015
Published online 22 APR 2015

A statistical study into the spatial distribution and dawn-dusk asymmetry of dayside magnetosheath ion temperatures as a function of upstream solar wind conditions

A. P. Dimmock[1], K. Nykyri[1,2], H. Karimabadi[3,4], A. Osmane[1], and T. I. Pulkkinen[1]

[1]School of Electrical Engineering, Aalto University, Espoo, Finland, [2]Department of Physical Sciences, Embry-Riddle Aeronautical University, Daytona Beach, Florida, USA, [3]University of California, San Diego, La Jolla, California, USA, [4]SciberQuest, Inc., Del Mar, California, USA

Abstract The magnetosheath contains the shocked solar wind and behaves as a natural filter to the solar wind plasma before it reaches the magnetosphere. The redistribution of kinetic energy at the bow shock results in significant thermalization of the solar wind plasma, resulting in a magnetosheath temperature profile which is highly nonhomogeneous and nonisotropic and differs between the dawn and dusk flanks. The present study attempts to study the spatial distribution of magnetosheath ion temperature as a function of upstream solar wind conditions. We pay particular attention to the dawn/dusk asymmetry in which we attempt to quantify using experimental data collected over a 7 year period. We also compare these data to simulated data from both the Block-Adaptive-Tree-Solarwind-Roe-Upwind-Scheme (BATS-R-US) MHD code and a kinetic hybrid model. We present evidence that the dawn flank is consistently hotter than the dusk flank for a variety of upstream conditions. Our statistical data also suggest a dependency on solar wind speed such that the level of asymmetry increases with faster speeds. We conclude that the dawn-favored asymmetry of the magnetosheath seed population is insufficient to explain the dawn asymmetry (30–40%) of cold component ions in the cold, dense plasma sheet, and therefore, other mechanisms are likely required.

1. Introduction

The supersonic solar wind (SW) is slowed to subsonic speeds when encountering the terrestrial magnetosphere (MSP), forming a standing shock wave upstream of the planet known as the bow shock (BS). The region immediately behind the BS is known as the magnetosheath (MS) and contains the "shocked" SW plasma which is hotter, denser, slower, and more turbulent compared to the upstream plasma. The MS extends to the magnetopause (MP), which is maintained by the pressure balance between the MS and the MSP plasma, thus dividing the two regions. The role of the MS can loosely be described as a natural interface between the SW and MSP regions and therefore is a fundamental component in driving plasma properties in the inner MSP.

Many studies have been devoted to the MS [e.g., *Spreiter et al.*, 1966; *Fairfield*, 1976; *Luhmann et al.*, 1986; *Petrinec et al.*, 1997; *Němeček et al.*, 2000; *Paularena et al.*, 2001; *Zastenker et al.*, 2002; *Longmore et al.*, 2005; *Verigin et al.*, 2006; *Soucek and Escoubet*, 2011; *Walsh et al.*, 2012; *Lavraud et al.*, 2013; *Dimmock and Nykyri*, 2013; *Nykyri*, 2013], which have been a combination of simulation-, theory-, and experiment-based studies. What is clear from the aforementioned literature is that the MS properties are subject to dawn/dusk asymmetries primarily formed (both directly and indirectly) from the orientation of the interplanetary magnetic field (IMF). To summarize these asymmetries, magnetic field strength and velocity are stronger on the dusk sector, whereas density, ion temperature, and magnetic turbulence are larger on the dawn flank [*Němeček et al.*, 2000; *Paularena et al.*, 2001; *Longmore et al.*, 2005; *Walsh et al.*, 2012; *Dimmock and Nykyri*, 2013]. These asymmetries have been observed under a Parker-spiral (PS) IMF orientation, and therefore, the dawn and dusk flanks correspond to a BS under a quasi-parallel ($Q_{\parallel}$) and quasi-perpendicular ($Q_{\perp}$) configuration, respectively. Although the BS geometry plays a critical role, the physical mechanisms driving and maintaining such asymmetries remain unclear. For example, MS temperature is a highly kinetic property which is a function of not just magnetohydrodynamic (MHD) processes but the array of instabilities and wave-particle interactions known to exist in the MS. In addition to this, certain processes such as Kelvin-Helmholtz instability (KHI) [*Chen et al.*, 1997; *Otto and Fairfield*, 2000; *Nykyri and Otto*, 2001; *Nykyri et al.*,

2006; *Hwang et al.*, 2011; *Nykyri*, 2013], flux transfer events (FTEs) [*Russell and Elphic*, 1979; *Sibeck*, 1990, 1992; *Sibeck and Smith*, 1992; *Nykyri et al.*, 2003], and subsolar magnetic reconnection *Dungey* [1961] can also play a role. For example, it was recently shown that KHI favors the dawn flank during a typical PS IMF orientation [*Nykyri*, 2013]. The problem is further complicated by upstream variations on short and large temporal scales. It was suggested by *Paularena et al.* [2001] that the dawn-favored density asymmetry present in their results was to some extent dependent on the current solar cycle. This could explain why *Dimmock and Nykyri* [2013] could not identify such an asymmetry from Time History of Events and Macroscale Interactions during Substorms (THEMIS) data collected between October 2007 and October 2013. The present study will concentrate entirely on the spatial distribution and asymmetry of ion temperature in the dayside MS. Recently, strong evidence of an ion temperature asymmetry has been suggested by *Walsh et al.* [2012] using THEMIS data and MHD simulations. However, the physical processes maintaining this asymmetry are still not completely understood. It has been proposed that any asymmetry of ion temperature in the MS could play a key role in driving plasma properties in the MSP [*Fujimoto et al.*, 1998; *Hasegawa et al.*, 2003, 2004, *Wing et al.*, 2005].

Fujimoto et al. [1998] used Geotail observations collected in the near-Earth tail flanks to address the problems associated with plasma transport across the low-latitude boundary layer (LLBL) and the subsequent impact on the formation of the plasma sheet. The presence of cold, dense ions in both the LLBL and the plasma sheet maintains the notion that MS ions are directly transmitted through the flanks into the MSP, and therefore, understanding the complex transport mechanisms is an area of particular interest to magnetospheric physics. In the study by *Fujimoto et al.* [1998], they observed an asymmetry in the ion data, where the energy of MSP and MS ions were distinctly separated on the dusk flank but indistinguishable on the dawnside. They attributed this asymmetry to the cross-tail magnetic drift of plasma sheet ions which would supply additional energetic ions to the duskside. Their data also suggested the direct transport of MS ions into the cold, dense plasma sheet from the near-Earth flanks, and the mechanism they proposed for capturing the cold, dense plasma was associated with magnetic reconnection. Although KHI was mentioned, it was believed that KHI mixing would have to be accompanied by other higher-frequency processes to make this a viable option.

Hasegawa et al. [2003] used Geotail data to study the characteristics of ion and electron signatures on the dayside MSP just inside the MP with the aim to better understand the formation of the LLBL. They noticed that during prolonged periods of northward IMF (NIMF), the mixing of the MSP- and MS-originating ions are clearly separated on the dusk flank but not on the dawnside. They proposed several reasons, the most relevant to this particular study being that (1) the heating of MS ions on the dawn flank could be higher than on the duskside and (2) there could be a dawn-favored asymmetry of wave activities in the MS. Regarding reason 2, recently, *Dimmock et al.* [2014] reported evidence that magnetic turbulence in the Pc 2 range was substantially larger on the dawn flank during PS and NIMF, which could contribute to heating on the dawn flank.

Soon after this, *Hasegawa et al.* [2004] performed an additional study but using a slightly longer Geotail data set ranging from November 1994 to December 1999. Their goal was to study the ion properties in the low-latitude boundary region in order to understand the mechanisms driving the cold, dense plasma sheet under extended periods of NIMF. They concluded that in the mixed ion region, ions originating from the MS remained cool on the dusk flank but, on the other hand, appeared significantly heated on the dawn. They also suggested that the nature of the plasma transport and heating processes may vary with different ranges of magnetic local time.

Wing et al. [2005] used data from the Defence Meteorological Satellite Program and IMP 8 to study the temperatures of the hot and cold component ions in the plasma sheet. These data were not collected in situ but mapped from ionospheric observations using the technique described in *Wing and Newell* [1998]. One of the significant conclusions from this study was that they observed a ~30 to 40% dawn-favored asymmetry of cold component ions in the plasma sheet. Interestingly, since the cold component ions are believed to originate from the MS, then one should observe a dawn-favored asymmetry in the MS as well. However, either the seed population of ion temperatures in the MS are indeed ~30 to 40% hotter or some additional heating mechanism takes place during transport or at the boundaries.

Yao et al. [2011] performed a statistical study using THEMIS data to investigate the role of electromagnetic fluctuations across the MP, concentrating on frequencies between 0.001 and 2 Hz. They reported larger

spectral energy densities of ion gyroradii scales on the dawn flank which showed no apparent dependence on the MS B_z component. Such an asymmetry could provide additional ion heating, which may play a role in elevating temperatures measured at the dawn flank and thus contribute to the asymmetry observed in the plasma sheet. They interpreted the role of these fluctuations as facilitating a large proportion of the plasma transport into the MSP.

Wang et al. [2012] used 4 years of THEMIS data to study the spatial distribution of the ion temperature (T_i), electron temperature (T_e), and the ion-to-electron temperature ratio (T_i/T_e) in the MS and plasma sheet. In their study, T_i/T_e increased by at least an order of magnitude moving from the SW → MS and MS → MSP. They also found a positive correlation between T_i/T_e and SW velocity stronger than any correlation performed on other upstream conditions. They observed a strong decrease in both T_i and T_e moving tailward from the subsolar point but simultaneously little variation in T_i/T_e. The authors attributed this to adiabatic cooling of the ions and electrons.

Walsh et al. [2012] used THEMIS data to perform a statistical study of the MS plasma properties in close proximity to the dayside MP. They analyzed 1114 dayside crossings between 2008 and 2010 and found a dawn-favored asymmetry of ion temperature which was 12% at its maximum. The authors also reported larger ion densities on the dawn flank and larger magnetic field strength and ion velocity on the dusk flank. They concluded that their observations were consistent with the results produced by the BATS-R-US global MHD code for similar upstream parameters.

The present study aims to shed light on the results by *Fujimoto et al.* [1998], *Hasegawa et al.* [2003], and *Wing et al.* [2005] and build on recent MS studies such as that by *Walsh et al.* [2012], in which strong evidence has suggested the presence of a dawn-favored ion temperature asymmetry in the MS. We specifically aim to address how any MS asymmetry compares with that in the plasma sheet, and how does this depend on upstream conditions. With the aid of MHD and global kinetic hybrid simulations, we will also attempt to identify whether the asymmetry is driven by kinetic-based, as opposed to MHD-based, processes.

This paper is structured as follows. Section 2 describes the data processing. Section 3 presents the results created for the complete database (CD), NIMF, southward IMF (SIMF), slow SW (SSW), and fast SW (FSW). We will follow section 3 with a discussion of the presented results, where we will attempt to put our data in context with the existing literature. We will finish this paper by drawing and summarizing our conclusions.

2. Data Selection and Processing

For the present study we utilize data originating from two different sources. THEMIS [*Angelopoulos*, 2008] measurements are used to compile our statistical database and make up the entirety of our MS data sets. To obtain the estimates of MS ion temperatures, we take directly the measurements supplied by the electrostatic analyzer instrument [*McFadden et al.*, 2008] on board each probe. The data sets we use are the L2 moments at the spin resolution (~3 s). We also require observations directly upstream of the BS nose, and for this we use the OMNI database (http://omniweb.gsfc.nasa.gov). The OMNI data are not collected in situ but measured at various upstream locations by several spacecraft and propagated to the BS nose [*King and Papitashvili*, 2005] based on the *Farris and Russell* [1994] BS model. We currently use the high-resolution 1 min OMNI data files. We also present simulated results produced by the BATS-R-US [*Tóth et al.*, 2005] global MHD model which is run via the Community Coordinated Modelling Centre (CCMC) (http://ccmc.gsfc.nasa.gov). As a sanity check, we also compare these results with runs from the Grand Unified Magnetosphere Ionosphere Coupling Simulation (GUMICS) MHD code [*Janhunen*, 1996; *Palmroth et al.*, 2005; *Janhunen et al.*, 2012]. These results were run locally using GUMICS-4 and are also available via CCMC. In addition, we present results from a global kinetic hybrid code [*Karimabadi et al.*, 2006, 2010, 2013].

For each THEMIS location initially in the geocentric solar ecliptic frame, we perform a transformation to the magnetosheath interplanetary medium (MIPM) reference frame [*Verigin et al.*, 2006]. The MIPM frame transformation allows for (1) planetary aberration, (2) changes in the BS geometry resulting from rotations of the IMF out of the PS, and (3) motion of the MS boundaries. In practice, the first is achieved by setting the MIPM x axis in the direction of the upstream plasma velocity vector. Prior to this, the Earth orbital velocity is subtracted from the y component of the SW plasma velocity. In our case, this is already implemented in the OMNI data set and so is unnecessary. The y axis of the MIPM frame is computed as a function of the upstream IMF vector which in effect organizes data points with respect to the geometry of the BS.

The purpose of this stage is so that MS measurements collected during different IMF orientations can be directly compared since they were processed by similar shock geometries. Motion of the MS boundaries are accounted for by computing the positions of each boundary during each upstream condition, which is then used to calculate a fractional distance (F_{mipm} = 0 MP] → 1 [BS]) across the model MS. F_{mipm} is used to determine when each spacecraft occupies the MS and also its relative (with respect to the boundaries) position within the MS. Each location in the MIPM frame consists of the fractional distance between the boundaries, a clock angle, and a zenith angle, which are defined on the *XY* and *YZ* planes, respectively. We use the *Shue et al.* [1998] and *Verigin et al.* [2001] MP and BS models to estimate boundary locations based on upstream estimates provided by the OMNI data. To determine the upstream SW conditions, we compute a 20 min average of the 1 min OMNI data to account for any uncertainties associated with the convection time from the BS nose to the spacecraft locations. In addition to this, to minimize the impact from transient features in the IMF resulting in inaccurate estimates of the IMF orientation, we remove data when the IMF cone angle variation exceeds 20° within each 20 min window. The limit of 20° appears to provide the optimal "trade-off" between the removal of statistical data and the presence of statistical noise in our results.

At each probe location, a 3 min windowed mean average is used to estimate the plasma parameters for each data point in the MS. The windowed average reduces the effect of small-scale perturbations and measurement errors yielding inaccurate estimations of plasma properties at each location. In addition, we transform each window into a unit-less quantity using a *z*-score. The *z*-score measures each window as a distance of the standard deviations (σ) from the mean. Only windows which meet the criterion $\sigma \leq 1$ are included in the final statistical database. As a result, when a particular plasma parameter experiences significant variations within a window, the mean average is not included in the statistical database. To prevent the inclusion of SW data in our MS data set, we impose a limitation which requires the MS plasma velocity to be less than that measured upstream. Misidentification of SW data can be the result of either inaccuracies associated with the BS model or errors in the estimates of upstream conditions, both of which are unavoidable and need to be addressed. Since we are only considering the dayside MS, flow speeds faster than the SW should be statistically insignificant. It should also be noted that existing studies have shown strong evidence of supersonic MS flows [*Hietala et al.*, 2012]. However, the occurrence of these events should be less frequent compared to typical MS conditions. Regarding misidentification of data associated with the MP, we remove obvious outliers which are clearly not measured within the MS. In practice, we remove data points which are very far from the typical distribution of MS values. In addition, to ensure that results are not directly caused by MP motion, we produce numerical estimations based on data collected in the middle of the MS and not close to each boundary.

From our MS databases, we create statistical maps (SMs) by binning each MS database into a grid on the MIPM *XY* plane. Each data point is allocated to a particular bin based on the [X_{MIPM}, Y_{MIPM}] coordinate of each data point. In this particular study, we apply a fixed grid space where each bin dimension is 0.5 × 0.5 Re. The bin dimension was chosen as 0.5 Re since it proved optimal based on providing adequate grid resolution, suitable bin density, and minimizing the statistical error. The value of each bin corresponds to the mean average of the plasma parameters within each bin. It should be noted that we produce the same SMs for median bin averages for validation purposes (not shown). More importantly, the conclusions presented in this study are independent of the bin averaging method. We refer to *Dimmock and Nykyri* [2013] for a more complete and comprehensive description of this methodology. Also see *Verigin et al.* [2006] for an alternate account of the MIPM frame and a detailed description of the boundary models.

In addition to the SM, we also create cross-sectional cuts using the MS statistical databases. The statistical cuts are plotted as a function of the MIPM zenith angle and are calculated by evaluating the mean of the plasma parameters within a sector of the dayside MS. The angular resolution of each sector is 15° (1 h), and we apply a 50% overlap of each sector. We eliminate the sector between noon and 1 h due to the lack of data coverage in this region. Local noon in the MIPM frame corresponds to very strong radial IMF when the spacecraft is located at local noon and therefore is statistically rare. As a result, many points at local noon are rotated away from this region since the IMF is statistically PS. The primary role of the statistical cuts are to obtain a more quantitative measure of the profiles of the MS plasma parameters and to show more delicate features not visible in the SM. Since the MS plasma parameters close to the MS boundaries are susceptible to large variations, in the current study we provide the numerical cuts for the middle third of the MS ($1/3 \leq F_{MIPM} \leq 2/3$) to avoid these turbulent regions.

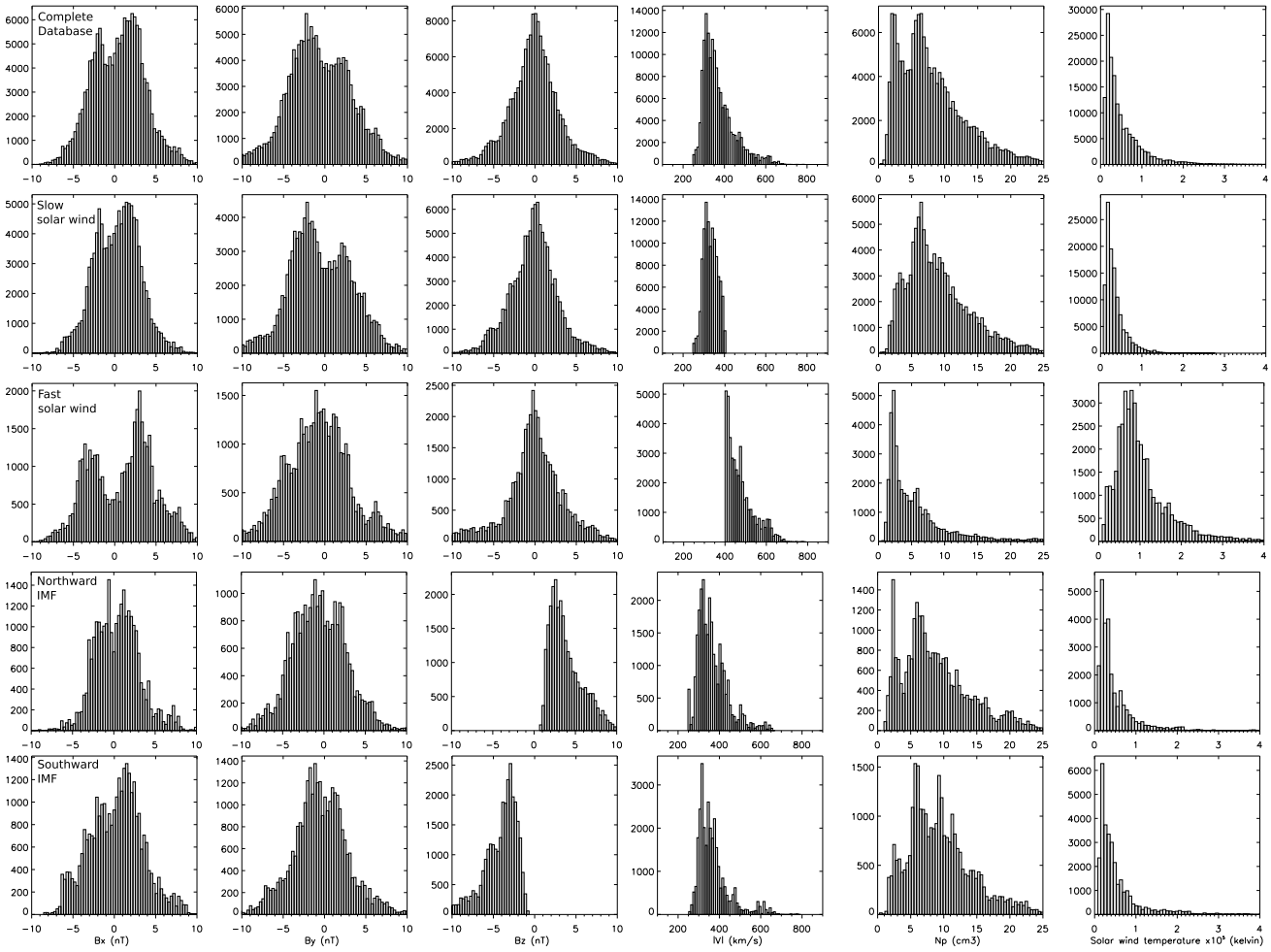

Figure 1. Distributions of solar wind parameters for the complete database, slow SW, fast SW, northward IMF, and southward IMF.

The above procedure for the production of the MS statistical data, SM, and numerical cuts can be replicated for various upstream conditions based on the OMNI data. In the current study we compare data for the CD, NIMF ($B_z > 0.5|\mathbf{B}|$) , SIMF ($B_z < -0.5|\mathbf{B}|$) , FSW (> 400 km/s), and SSW (< 400 km/s).

3. Results

3.1. Solar Wind Statistics

Presented in Figure 1 are the distributions of SW parameters for each compiled MS database. Each panel represents a set of upstream conditions corresponding to each individual MS database. Typical SW conditions (complete database) are approximately $|B| = 4$ nT, $|V| = 350$ km/s, $M_a = 7.5$, $M_{ms} = 5$, $T_i^{sw} = 2.5 \times 10^4$ K, $N_p = 6.5$ cm^{-3}, and the multiple bumps seen in the distributions of B_x and B_y correspond to inward and outward PS IMF. The remaining data sets for SSW, FSW, NIMF, and SIMF are in the panels below, in which the individual filtering of the data becomes obvious. There are two differences to point out which arise due to the filtering of the CD. First, larger SW temperatures and lower densities are associated with the FSW, whereas the opposite is true for SSW data. Second, the PS nature of the IMF is absent from the NIMF and SIMF databases as expected. Importantly, neither of the distributions imply any notable (unintentional) statistical bias, and to be thorough, we also reproduced these distributions separately for the dawn and dusk flanks, and the same case is true. As a further check, we did the same as a function of magnetic local time, and similar to before, we observed no reason to suggest that any of our results are generated by an artificial element. These distributions are plotted in Figure A2. Any discrepancies that we observed are discussed in section 4 in context with their physical significance.

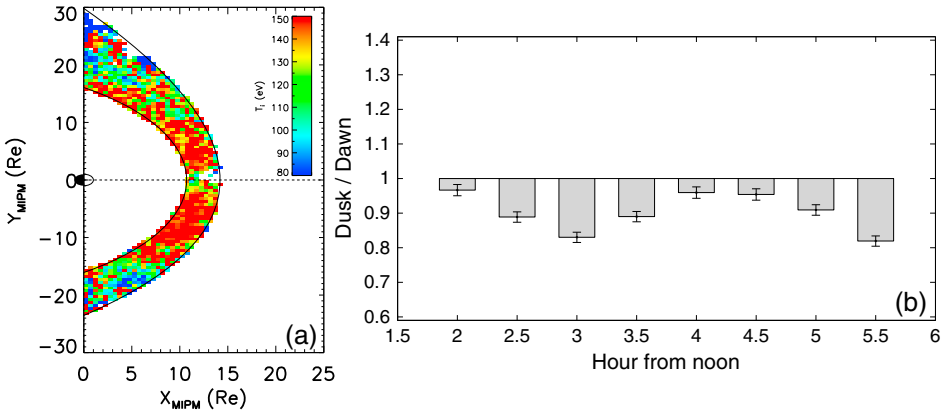

Figure 2. (a) Statistical map and (b) dusk/dawn ratio for the complete database.

3.2. Complete Database

The SM of T_i for the CD is presented in Figure 2a, whereas the profile of dusk/dawn ratio is plotted in Figure 2b. In Figure 2b, the error bars are determined by the maximum variation resulting from the standard error of the mean (SEM) $= \sigma / \sqrt{n}$. The individual profiles of the dawn and dusk flanks (for each SW criterion) are subsequently plotted by the various colored lines in Figure 7, where the black line corresponds to the CD. Values of T_i are largest at the subsolar region (>150 eV), but afterward there is a tendency for T_i to steadily decrease in the tailward direction to ~130 eV and ~100 eV on the dawn and dusk flank terminators, respectively. The dusk/dawn ratio presented in Figure 2b suggests a dawn-favored asymmetry in which the individual values vary between a minimum and maximum of 3.3% and 18.1%, respectively, and the mean is ~9.8%. The asymmetry is also present in Figure 2a (particularly between 2 and 4 h), but due to its delicate nature, a more reliable and quantitative estimate is provided by Figure 2b. The maximum asymmetry is present at 3 h, but no obvious pattern is associated with the spatial distribution. To assess the statistical significance, SM of bin density and statistical error can be found in the first column on Figure A1. The bin density is typically >300 points per bin, and the standard error is between 5 eV and 8 eV. The isolated points of increased error on the $Q_{\parallel}$ shock is likely due to the increase in turbulence and instabilities that are abundant downstream of the shock front. MHD simulations produced by the BATS-R-US global MHD code under similar SW conditions are shown in Figure 8a. Comparable to the SM in Figure 2a, the spatial distribution is consistent, where hotter temperatures are located in the subsolar region and then decreases toward the terminator. Contrary to the SM in Figure 2a, no obvious dawn-favored asymmetry appears to manifest in the MHD run.

3.3. Slow SW

Figure 3 is plotted in the same manner as Figure 2 but in this case for the SSW data set. The same dawn and dusk profiles for SSW are now represented by the blue lines in Figure 7. The similar spatial distribution of T_i is

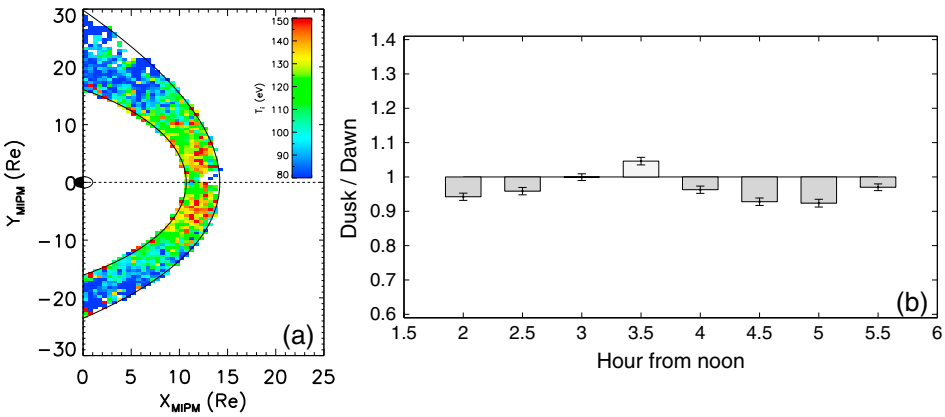

Figure 3. (a) Statistical map and (b) dusk/dawn ratio for the slow solar wind database.

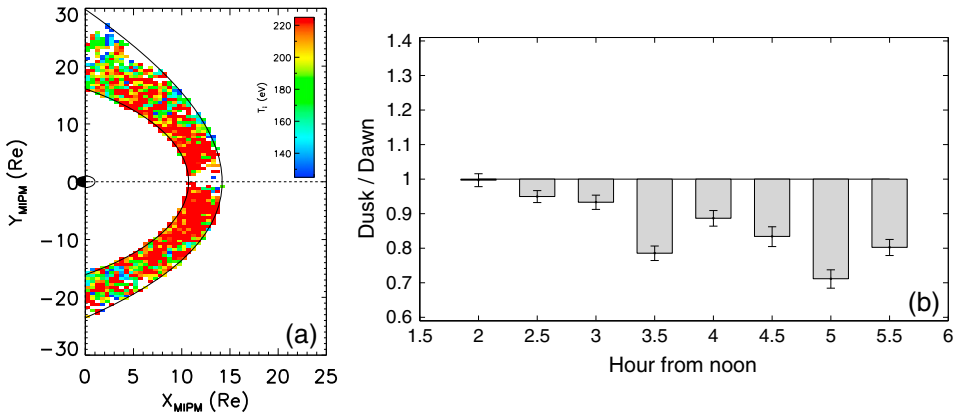

Figure 4. (a) Statistical map and (b) dusk/dawn ratio for the fast solar wind database.

still observed with the hottest values recorded in the close vicinity of the subsolar region, which then cools in the tailward direction. At the subsolar region, ion temperatures are approximately 130–140 eV and cool to less than 100 eV at the terminator. Comparing the SM and cross-sectional profiles to those in Figure 2, the MS during SSW conditions is visibly "cooler." In fact, the values of T_i during SSW are the least when comparing any of our data sets. The decrease in T_i for SSW conditions are consistent with the Rankine-Hugoniot conditions [*Kulsrud*, 2005]. Whereas the increase in magnetic pressure is constrained by a factor of 16 for very high Mach numbers, the temperature increase in a collision-less shock is unbound. It is worth noting at this point that although T_i is visibly reduced, our statistical data still suggest the presence of a dawn-favored asymmetry, albeit lesser. The asymmetry is not obvious from Figure 3a and is only observable in the numerical data in Figure 3b. The mean asymmetry is estimated at 4.5%, where the individual maximum and minimum values are 7.6% and 0.1%, respectively. It is obvious from these moderate estimates why the asymmetry may not be visible from the SM. There appears to be no obvious spatial distribution to the asymmetry with the exception of a decrease in the dawn-favored values, and then surprisingly, a dusk-favored asymmetry is present around 3–3.5 h and 5.5 h. This particular observation is counter to the CD, but the remaining regions show a relatively consistent dawn-favored asymmetry that is approximately 5%. The simulated MS in Figure 8b also confirms that the MS is cooler when the upstream plasma velocity is reduced. The reduction of T_i is not as striking as in the observational data. However, this may be due to the fact that our SSW database contains an array of upstream speeds, some of which are less than the value chosen for the simulation run (300 km/s). In this data set, the data coverage is reduced slightly but still remains in excess of 200 points per bin. The standard error is notably reduced, implying that the variation of T_i during SSW conditions also decreases. The standard error in this case is between 2 eV and 4 eV and varies little from this range. The reduction in error could be explained by the decrease in the amplitude of magnetic turbulence during SSW speeds [*Dimmock et al.*, 2014].

3.4. Fast SW

The SM and dawn/dusk ratios (with a similar format to the previous sections) are plotted in Figure 4 for FSW conditions, and the red lines in Figure 7 correspond to the dawn and dusk profiles. It is immediately clear that during FSW conditions, the values of T_i in the dayside MS are visibly enhanced. It is worth noting that the color scale in Figure 4a is offset to accommodate the larger magnitudes of T_i. The increase of T_i is also evident from the red line plotted in Figure 7, which noticeably exceeds any other dawn and dusk profile. Values of T_i measured at the subsolar region are typically 280 eV and 220 eV at the terminator. Around 3 h from local noon, T_i are approximately 75% larger than the CD and almost twice those compiled for the SSW data set. Interestingly, our statistical data still suggest the presence of a dawn-favored asymmetry which varies between a minimum of 0.2% (2 h) and a maximum of 28.8%. The mean asymmetry is estimated to be 18.7%, which is substantially larger than the previous estimates for the CD and SSW. It should also be noted that this value also exceeds any estimates for the remaining NIMF and SIMF data. The MHD run in Figure 8 is consistent with the SM in the sense that T_i is hotter during FSW conditions. As with the previous MHD runs, there is little evidence of a dawn asymmetry or its enhancement in the region we produce our cuts. Regarding the statistical significance of our results, the bin density is ~100 points per bin between 2 and 4 h

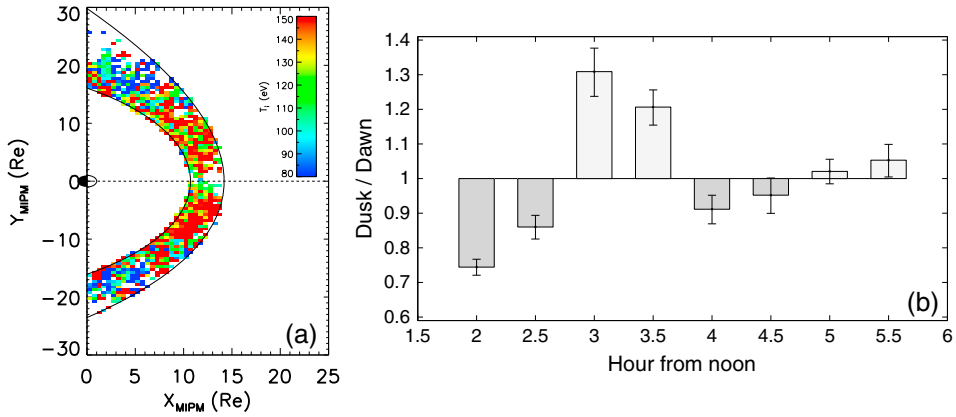

Figure 5. (a) Statistical map and (b) dusk/dawn ratio for the northward IMF database.

and then decreases to approximately 25 at the terminator. Statistical error has increased and now ranges between 5 eV and 10 eV. The increase in the standard error with SW speed is expected by the enhanced values of T_i and the larger-amplitude turbulence prevalent during FSW. The dawn and dusk distributions in Figure A2 show slightly higher counts on the dawnside for moderate SW speeds. This could contribute to the additional asymmetry but is unlikely especially considering we observed a reduction in asymmetry also by reducing SW speed. Nevertheless, the reported asymmetries lie within the estimated standard error indicated by the error bars in Figure 7.

3.5. Northward IMF

The SM and dusk/dawn ratio plots for NIMF are located in Figure 5, and the profiles of each flank are represented by the green lines in Figure 7. Two hours from noon, the typical values of T_i are ~200 eV on the dawn flank and 150 eV on the dusk. T_i then gradually decreases tailward to values around 100 eV at the terminator. The values of T_i are comparable with the values for the additional data sets but are still less than the FSW case. Interestingly, on the dusk flank 3 h from noon, there is a notable increase in T_i which is not reflected in the dawn flank. As a result, this creates a significant dusk-favored asymmetry in these isolated regions which is around 30%. With the exception of the region between 3 and 3.5 h, there is still evidence supporting a dawn-favored asymmetry as reported in the previous data sets. The minimum, maximum, and mean asymmetries are estimated as 4.7%, 25.7%, and 13.3%, respectively. The MHD data for NIMF can be found in Figure 8. Similar to the previous data sets, the MHD run is similar in its spatial distribution with the exception that the simulated data lack a dawn/dusk asymmetry. The typical bin density (closer to the MP) between 2 and 3 h is ~75–100 points per bin. The regions tailward from 3 h possess bin densities of around 20 points, but at the terminator this further decreases. We will avoid drawing conclusions which are tailwind

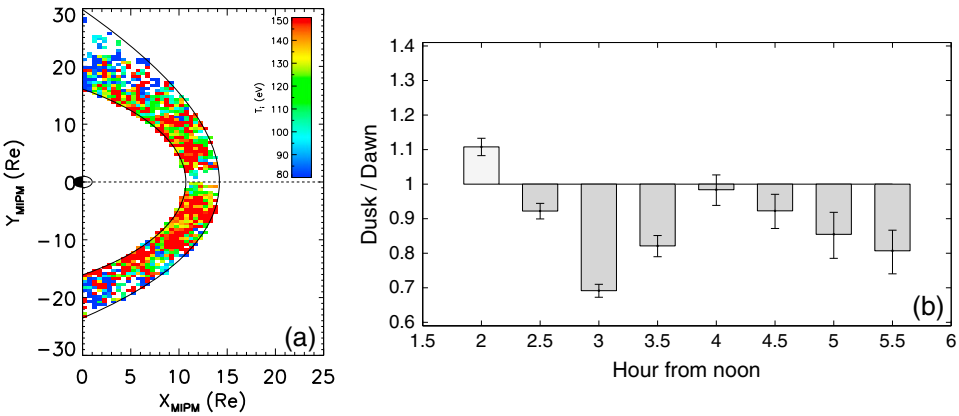

Figure 6. (a) Statistical map and (b) dusk/dawn ratio for the southward IMF database.

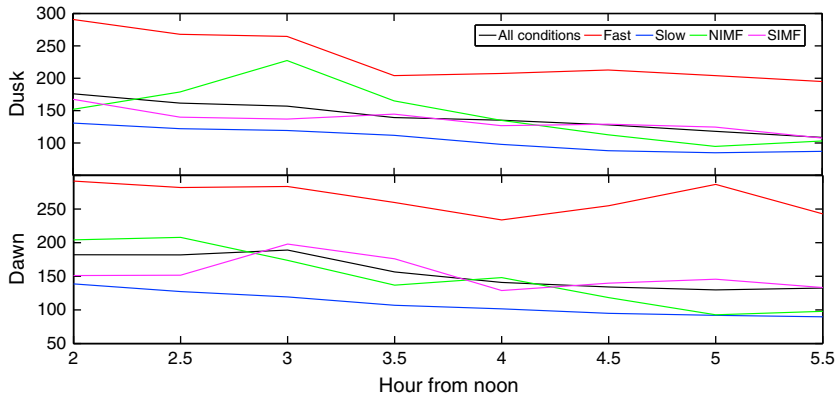

Figure 7. The profile of ion temperatures in the dayside MS as a function of hours from noon. (top) The dusk flank and (bottom) dawn flank values. Each color is plotted for each upstream criterion used to create the statistical maps.

further than 3 h due to this reason. The standard error is between 6 eV and 8 eV with isolated values higher and lower than this.

3.6. Southward IMF

Figures 6a and 6b represent the similar SM and asymmetry estimation as the preceding data sets. The magenta line in Figure 7 shows the profile of SIMF dawn and dusk data. Typical values of T_i during SIMF are approximately 160 eV in the subsolar region and 120 eV at the terminator. Figure 6b implies strong evidence of a dawn-favored asymmetry consistent with the previous results. Although initially there is a dusk-favored asymmetry, the remaining data stay dawn favored. The minimum, maximum, and mean symmetries (dawn favored) are estimated to be 1.6%, 30%, and 14.2%, respectively. Interestingly, on the dawn flank around 3–3.5 h there is an increase in T_i, as shown by the magenta line in Figure 7, which manifests as an elevated dawn-favored asymmetry. What is particularly worth noting here is that this increase of T_i on the dawn flank during SIMF corresponds to the same increase on the dusk flank during NIMF at the same corresponding location. The MHD runs presented in Figure 8 also exhibit a similar global MS profile for T_i. However, there

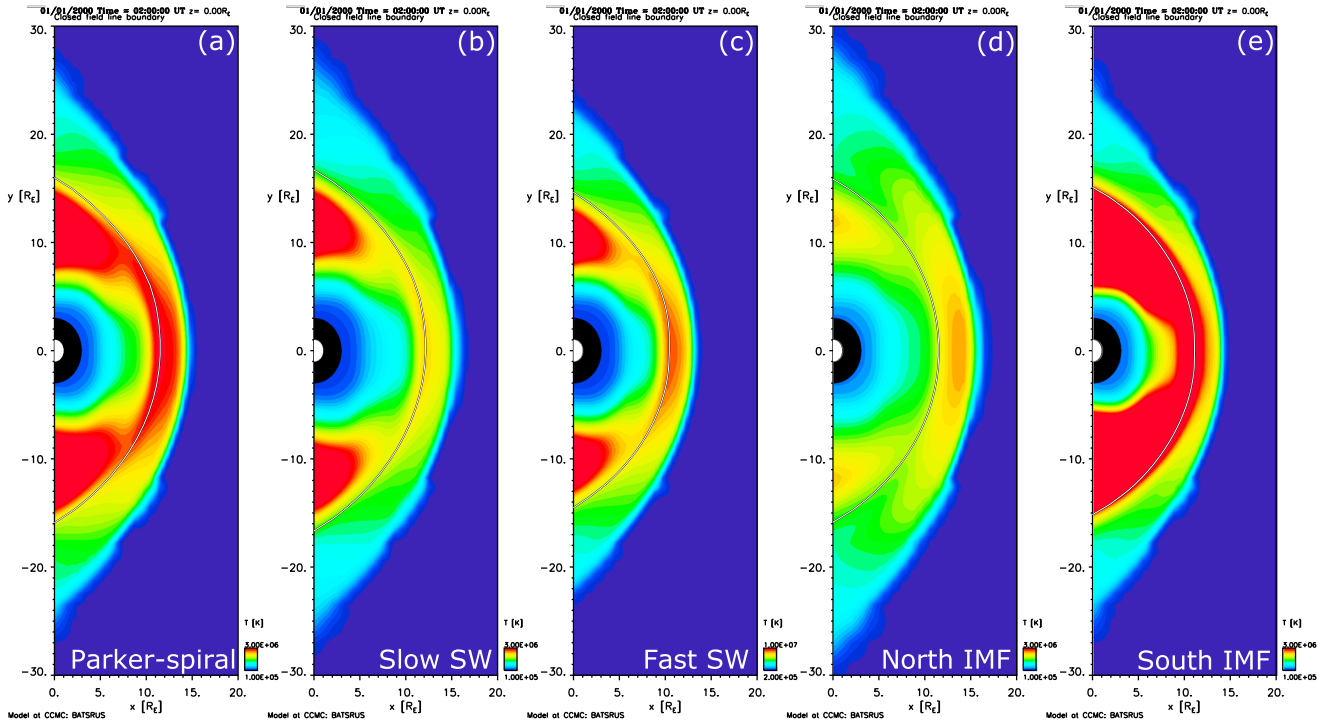

Figure 8. MHD runs produced by the BATS-R-US MHD code for (a) PS, (b) slow SW, (c) fast SW, (d) northward IMF, and (e) southward IMF.

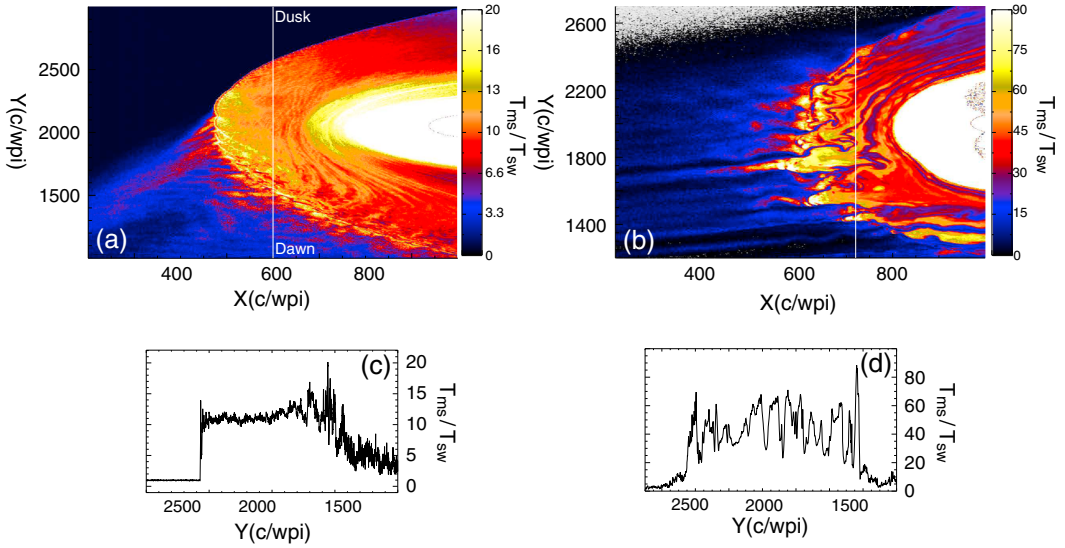

Figure 9. Examples from two simulations from the global hybrid kinetic model H3D. (a) Typical SW conditions but using an Alfvén Mach number of 5. (b) A run recently studied by *Karimabadi et al.* [2014], where the IMF is initially at −45° but is switched after 90 ion cyclotron inverse time to 10°. (c) Cross-sectional cut along the vertical white line in Figure 9a. (d) Cross-sectional cut along the vertical white line in Figure 9b.

is no evidence to suggest a dawn/dusk asymmetry similar to the other runs. In the simulated environment, there are no significant changes in temperature values between NIMF and SIMF, which is also consistent with the statistical data. From Figure A1, bin densities are 60 points per bin (subsolar), which decrease to around 10 points between 4 and 5 h and then significantly reduce at the terminator. Between 2 and 4 h the standard error is around 5 eV, which then increases at the MP around 4 h from noon to around 10 eV. All estimations of asymmetry are within the bounds of error, but we ignore data past 4 h due to low bin counts.

3.7. Global Hybrid Simulations

Presented in Figure 9 are global hybrid simulations of MS temperature under two distinct upstream conditions. In Figure 9a the $Q_{\parallel}$ shock can be identified from the pronounced foreshock, which is visible upstream in the lower half of the plot. The $Q_{\parallel}$ shock is also significantly more turbulent, which is expected from the abundant measurements of the $Q_{\parallel}$ shock transition. In each panel, a cut is taken and shown underneath each run. Each cut corresponds to the white vertical line shown in Figures 9a and 9b. The runs are created using the code H3D [*Karimabadi et al.*, 2006, 2010, 2013], which is a massively parallel hybrid code with stretched mesh capability. Using this code, a detailed study of the MS turbulence and its global consequences was recently conducted [*Karimabadi et al.*, 2014]. Here we show examples from two simulations focused on the issues associated with temperature asymmetry in the MS. Distances are normalized to ion skin depth (d_i), time is normalized to ion cyclotron frequency (X_{ci}), magnetic field is normalized to upstream magnetic field (B_o), density is normalized to upstream density (N_o), and velocity is normalized to the Alfvén speed ($V_A = B_o/\left(4\pi N_o m_i\right)^{1/22}$), where m_i is the ion mass. The first run shown in Figure 9a has β_i=0.7, β_e=1.9, $M_A = 5$, and IMF at 45°. The temperature is shown at $\Omega_{ci}t = 375$. This run is more comparable to the SM and the MHD runs, albeit with a lower Mach number. The profile in this case is much more locally homogenous, and a dawn-favored asymmetry which is approximately 10–15% is clearly present. This value is estimated from the cut in Figure 9c. The second run shown in Figure 9b has an Alfvénic Mach number ($M_A = V_{sw}/V_A$, where V_{sw} is the solar wind speed) $M_A = 8$, MP standoff position D_p=100, $\beta_e = \beta_i = 0.5$, and $\Omega_{pi}/\Omega_c i = 6000$. The IMF is initially at −45° but is switched after 90 ion cyclotron inverse time to 10°. Figure 9b shows a plot of total ion temperature, normalized to far upstream temperature, at $\Omega_{ci}t = 390$. Although the general profile of T_i remains (hotter values at the subsolar region and then decreasing tailward), the profile is extremely turbulent and nonstationary. Although from Figure 9b it appears that some dawn-favored asymmetry may be present, the cross-sectional cut displayed in Figure 9d is very turbulent, and therefore, any asymmetry cannot be accurately determined. The quantification of the asymmetry from the hybrid run would require a statistical approach. That means one would need to run multiple runs for various conditions, over extended periods of times, and then assume that the space average would be equal to the time

average (ergodicity). Such a methodology is beyond the scope of this report, but it is worth mentioning for future work and for highlighting the complexity of the MS plasma. The relevance of these results to the SM and MHD runs will be discussed further in the following section.

4. Discussion

The purpose of the present paper is to shed light on the previously reported dawn/dusk ion temperature asymmetry in the terrestrial MS using a combination of experimental and simulated data. We applied our statistical mapping tool to create SM of the ion temperature in the dayside MS for our complete database, SSW (< 400 km/s), FSW (> 400 km/s), NIMF, and SIMF. We also produced cross-section cuts as a function of hours from local noon for the same conditions to provide a more quantitative estimate. For similar upstream conditions, we also produced MHD runs using the BATS-R-US global MHD code to compare with the statistical data. Our main goals were to first quantify the magnitude of the asymmetry and determine if it could be responsible for the 30–40% ion temperature asymmetry reported in the cold, dense plasma sheet by *Wing et al.* [2005]. Second, we used the various data sets in order to resolve the level of dependence between the asymmetry and upstream SW conditions. Finally, we compared our statistical data with simulation runs from MHD and kinetic hybrid models to distinguish between the roles of MHD and kinetic processes.

In all of our statistical data sets we observed strong evidence that ion temperatures on the dayside dawn flank are visibly hotter compared to those on the dusk. The magnitude of the asymmetry varies between the data sets, but for typical upstream conditions, our data shown in Figure 2 suggested an average asymmetry of ~9.8%. For each of our statistical data, we failed to produce the same level of asymmetry in the MHD simulations. It should be said that MHD can generate a temperature asymmetry as reported by *Walsh et al.* [2012] in which larger density and temperatures on the dawn flank arise to balance the differences in magnetic pressure due to the asymmetric magnetic field strength on both flanks. *Walsh et al.* [2012] compared THEMIS data collected at the dayside MP to simulated data in the same region from the BATS-R-US global MHD code. Their observations reported a maximum asymmetry of 12%, whereas in the MHD data it was almost 30% at its maximum. Comparing the spatial distribution of the asymmetries provided by the observations and the MHD runs, there were also some discrepancies in the form of conflicting estimates as a function of hours from noon. For example, their maximum asymmetry of 12% was observed at 0–1 h from noon; however, the MHD run for the same region experienced no asymmetry at all. In general, the MHD runs appeared to overestimate the level of asymmetry favored by the dawn flank. It should be noted that these data were only collected in close proximity to the MP and between 2008 and 2010 and therefore is inherently different to the present study and thus difficult to compare directly. However, the point we make is that although MHD simulations can create an asymmetry of ion temperature, there remain unanswered questions regarding how dominant these MHD effects are and to what extent kinetic processes also contribute. In the present study we focused on data in the central MS to attempt to quantify the seed population and also to avoid complications associated with collecting data close to dynamic boundaries. When we compare our results for each set of upstream conditions with their corresponding MHD runs, the MHD runs do no appear (by visual inspection) to produce any significant asymmetry in the central MS. There are indications of slight asymmetries close to the MP created by the reasons previously stated, but by visual inspection there is nothing comparable with the statistical data. It is also possible that since our MHD input parameters differ to those by *Walsh et al.* [2012], then the asymmetry in our runs is weaker. Evidence of this is the reduced asymmetry of MS thickness in our runs. We do not imply that the MHD-generated asymmetry is absent from the observational data, but based on the discrepancies in past observations, and those in the present study, MHD does not complete the picture, and therefore, other mechanisms acting on much smaller timescales (smaller than the ion gyroperiod) likely play a role. This last point is evidenced by studies of mirror modes indicating that the MS plasma, and more specifically the ion temperatures and beta plasma, is often regulated by mirror-mode saturation processes [*Soucek et al.*, 2008; *Génot et al.*, 2009; *Balikhin et al.*, 2009]. Due to the plethora of processes inexistent in global MHD simulation present in the real system such as KHI, kinetic Alfvén waves (KAW), FTEs, mirror-mode instability/saturation, ion cyclotron instabilities/saturation, and enhanced magnetic field turbulence (which is stronger on dawn flank), it is logical to conclude that these kinetic processes will play a role in dictating the MS ion temperatures. This argument is also strengthened by the fact that KHI and higher-amplitude magnetic field turbulence favor the dawn flank during a typical PS IMF [*Nykyri*, 2013; *Dimmock et al.*, 2014]

conditions. To what extent kinetic process impact the MS ion temperatures involve complex wave-particle interactions which are beyond the scope of this report, but neither our studies nor that of *Walsh et al.* [2012] provides satisfactory justifications that MHD exclusively explains the observed dawn/dusk ion temperature asymmetry.

To shed further light on the role of MHD and kinetic processes, we also provided two kinetic hybrid simulation runs shown in Figure 9. The first Parker-spiral run also suggested a dawn-favored asymmetry of approximately 10–15%, depending on where the estimate was taken. By comparing the MHD runs with the kinetic simulations, the kinetic nature of MS temperature becomes apparent, and although both show similar global profiles, the kinetic runs and the observational data imply that the MS temperature is affected by processes on smaller scales than global MHD can resolve. The second run showed an extreme case [see *Karimabadi et al.*, 2014] in which the IMF switches from ortho Parker spiral to weakly radial (10°). The purpose of this run is to demonstrate that under dynamical upstream conditions, the MS temperature becomes highly nonlinear, and since the SW is continually changing, future work involving observations, MHD, and kinetic runs such as these are required to fully understand the impact from such conditions.

It was briefly mentioned above that enhanced turbulence [*Dimmock et al.*, 2014] and KHI [*Nykyri*, 2013] will favor the dawn flank during a PS IMF and as a result may contribute to the dawn-favored asymmetry observed in the data. It has been well documented [*Fairfield and Ness*, 1970; *Luhmann et al.*, 1986; *Zastenker et al.*, 2002; *Němeček et al.*, 2002; *Shevyrev and Zastenker*, 2005; *Shevyrev et al.*, 2006, 2007; *Dimmock et al.*, 2014] that the amplitude and intensity of magnetic field fluctuations are enhanced on the $Q_{\parallel}$ flank compared to the $Q_{\perp}$. The presence of the additional turbulence may enhance ion temperatures via wave-particle interactions. This interpretation is further supported by our recent observations [*Dimmock et al.*, 2014] where fluctuation amplitudes increased with solar wind speeds corresponding to larger asymmetries during similar upstream conditions as shown in Figure 4. Regarding KHI, during a PS IMF, the tangential magnetic field along the MP is weaker, which means that the dawn flank MP is statistically more unstable to KHI [*Nykyri*, 2013]. This may lead to more plasma heating at the dawnside flank associated with reconnection in KH vortices [*Nykyri et al.*, 2006; *Nishino et al.*, 2007], heating via plasma waves associated with KHI (such as KAW created by mode conversion [*Johnson et al.*, 2001; *Johnson and Cheng*, 2001]) or heating via shocks associated with KHI. However, it should be mentioned that KHI (and associated processes) are likely to only enhance ion temperatures within close proximity to the MP and are unlikely to be responsible for strong dawn-favored asymmetries observed far from the MP. Since we focus on the central MS, it is doubtful that KHI is capable of driving the asymmetry observed in our statistical data.

The data plotted in Figure 4 imply that as the SW speed increases, then the magnitude of the dawn-favored asymmetry also increases. In fact, as a general trend the MS temperatures on both flanks are significantly enhanced during faster SW speeds. Although the distribution of SW temperature are skewed to larger temperatures during faster speeds, this property is unlikely capable in driving hotter MS temperatures to the degree of what is observed. It should also be noted that the increase in temperature is also observed in the MHD run shown in Figure 8c, and even though the MSP was more compressed, there was still little difference between the dawn and dusk flanks. These results are evidenced by *Wang et al.* [2012] in which they reported that faster SW speeds resulted in larger values of $\frac{T_i}{T_e}$ and the dependence on SW speed was greater than any other IMF parameter they tested. Since ions undergo greater heating at the shock front compared to electrons [*Feldman et al.*, 1983], then this coincides with an increase of T_i consistent with the observations in this study. The fundamental process at the BS is to redistribute the kinetic energy of the SW bulk flow [*Sagdeev*, 1966; *Sagdeev and Galeev*, 1969; *Papadopoulos*, 1985], and when the SW speed increases, the BS is required to redistribute this additional kinetic energy and momentum. This leads to additional dissipation mechanisms driving higher-amplitude turbulence which could manifest as elevated ion temperatures measured downstream of the $Q_{\parallel}$ shock.

It was also shown in Figures 5 and 6 that during NIMF and SIMF, there are still indications of a dawn-favored asymmetry. We would not expect to measure a dawn/dusk asymmetry in the MS during NIMF and SIMF due to the symmetrical nature of the bow shock during these intervals. We interpret the presence of the dawn-favored asymmetry in Figures 5 and 6 as a temporal effect from when the IMF was PS. In effect, the dawn-favored asymmetries we are observing may well be remnants of the MS plasma which was processed when the IMF was PS. In addition, since the IMF never has zero B_x and B_y values, the dawn and dusk flanks are not strictly symmetric in terms of shock geometry. This fact could imply that a small asymmetry is still

generated even though then the SW is strongly northward or southward. It should also be mentioned that during NIMF we recorded slightly higher counts of hotter temperatures on the dawnside, and therefore, this may contribute to the asymmetries reported. If the above interpretation is inaccurate, then this would imply that the IMF does not strictly control the asymmetry and other factors should be considered. Nevertheless, in the real system when the IMF is either northward or southward, unless these intervals are sufficiently prolonged, then some temporal effect may be present in which a previous IMF orientation still dictates the plasma conditions. Therefore, any sufficient dawn-favored asymmetry already present in the MS may take time to dissipate or convect when the IMF switches away from a PS.

Based on studies conducted in the plasma sheet [*Fujimoto et al.*, 1998; *Hasegawa et al.*, 2003; *Wing et al.*, 2005], it was suggested that a MS temperature ion asymmetry was likely, but to what degree was unclear. The estimate of a 30–40% dawn-favored temperature asymmetry in the cold, dense plasma sheet during NIMF was provided by *Wing et al.* [2005]. It was discussed that this asymmetry could to a certain extent originate from the MS ion population. Our statistical data suggest that there is a dawn-favored temperature asymmetry in the MS, which is present in all of our data sets. For NIMF, the maximum was 27.5%. It should be said that 27.5% is not representative of the MS and a more reasonable estimate is the average of 13%, which is substantially less than the 30–40% predicted in the plasma sheet. The magnitude of the dawn-favored asymmetry observed in our statistical data varies between ~5% and ~15% and shows some dependence on upstream conditions, particularly the SW speed. Although we suspect that the IMF orientation plays a role in the driving of MS ion temperatures, this dependency is complex due to the various processes favoring certain orientations (eg., FTE, KHI, and reconnection) and different flanks. Importantly, our results show inconsistencies with MHD, and therefore, we propose that a more dominant role is performed by kinetic processes for driving ion temperature in the MS. One final conclusion to draw from these results is that a dawn-favored asymmetry in the MS seed population is present but unlikely to produce the 30–40% reported by *Wing et al.* [2005] in the plasma sheet. We suggest that additional mechanisms either in the vicinity of the MP or during transport are to likely account for the remaining temperature increase. The tasks of identifying these processes and quantifying their contribution require further study.

5. Conclusions and Summary

The present study has attempted to provide the first in-depth statistical study directly focused on quantifying the dawn/dusk asymmetry of ion temperatures in the dayside magnetosheath. In our investigation we used a synergy of observations, global MHD simulations, and global kinetic hybrid simulations. Based on our results we draw the following conclusions.

1. The dawn flank of the MS during a Parker-spiral IMF orientation is approximately 10% hotter during typical upstream conditions.
2. The magnitude of the dawn-favored asymmetry increased with solar wind speed, which results in an asymmetry estimated around 19%.
3. Discrepancies between the observations and MHD simulations in the present study and those shown by previous investigations suggest that MHD processes do not completely control the ion temperature asymmetry and other processes should play a role.

We conclude that the dawn magnetosheath flank is typically around 10–15% hotter than the duskside but varies depending on the upstream conditions. The solar wind speed plays a significant role where faster speeds result in a hotter and more turbulent profile, which seems to enhance the asymmetry. Although the present study has made progress on quantifying the magnetosheath temperature, the exact mechanisms responsible for generating and maintaining the asymmetry (particularly under a non-Parker-spiral IMF) remain unclear. We conclude by stating that although MHD processes can theoretically explain why a dawn-favored asymmetry may exist, the discrepancies in previous studies and those outlined in the present paper suggest that the kinetic processes on smaller scales than MHD are likely to contribute. To what extent MHD and kinetic processes are responsible requires further study and may be the focus of future publications.

Appendix A: Supplementary Statistical Maps

Figure A1 below shows the data coverage (top row) and statistical error (bottom row) for each of the upstream condition presented in the results above. The corresponding data set is indicated in each panel.

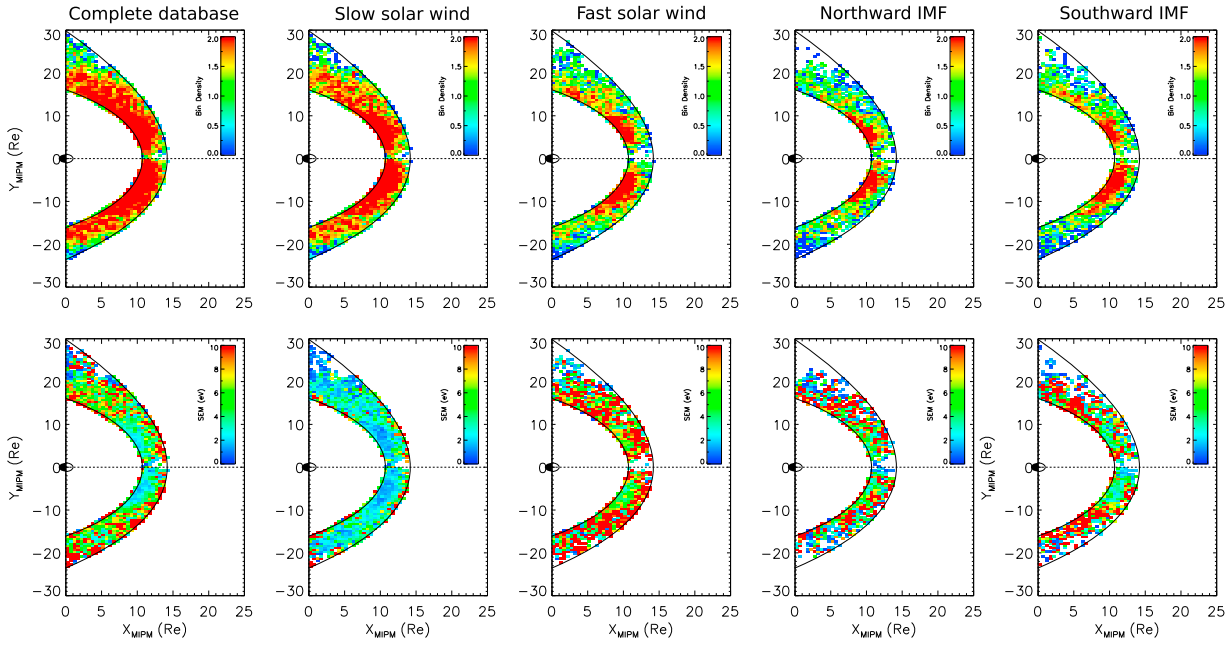

Figure A1. (top row) Statistical maps of bin density and (bottom row) statistical error of the mean. The bin density is plotted on a Log_{10} scale.

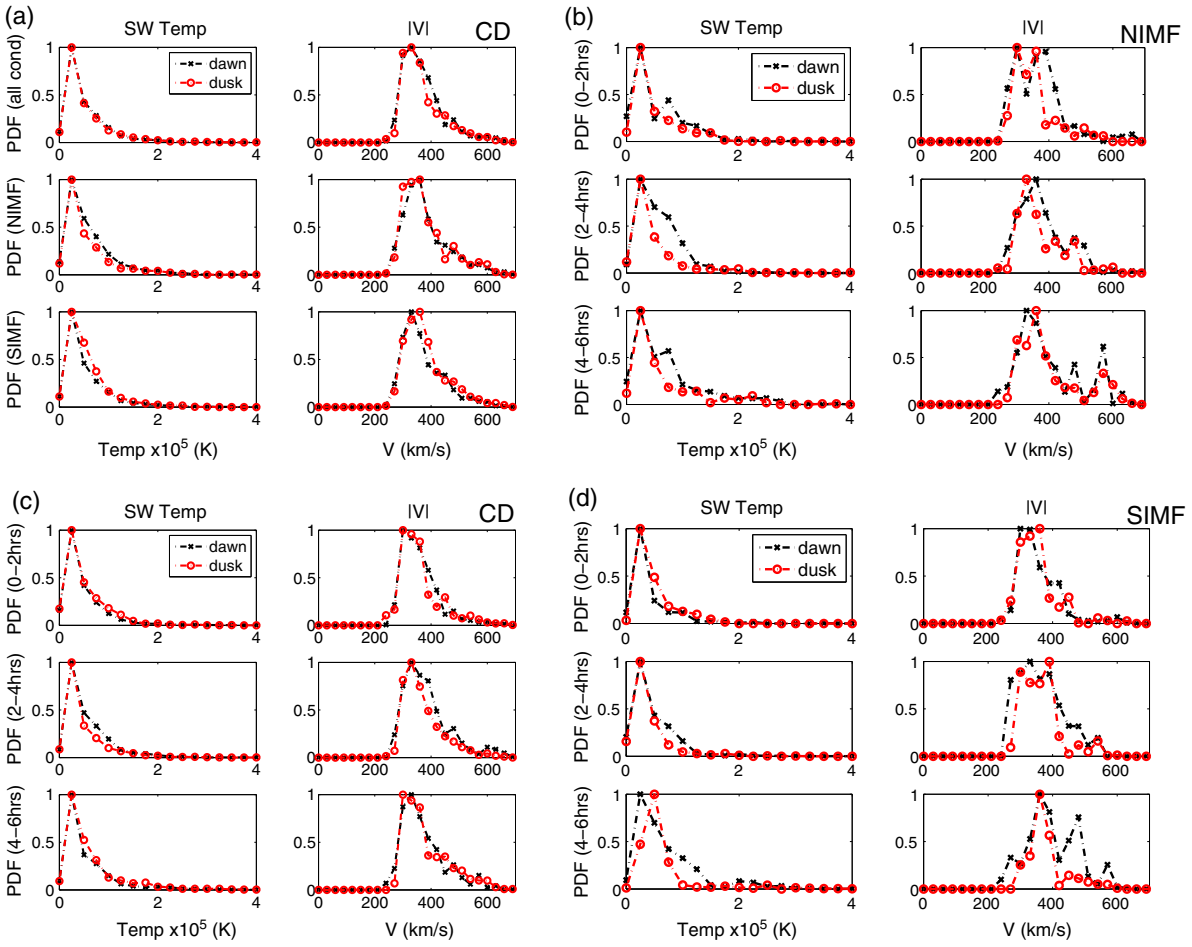

Figure A2. (a–d) Normalized probability density function (PDFs) of the solar wind velocity and temperature which correspond to the magnetosheath data collected on the dawn (red) and dusk (black) flanks. These distributions are shown as a function of hours from noon.

Acknowledgements
The work by A. Dimmock and K.Nykyri was supported by the NSF grant 0847120 and the Academy of Finland grant 267073/2013. The OMNI data were obtained from the GSFC/SPDF OMNIWeb interface at http://omniweb.gsfc.nasa.gov. The authors would also like to thank the THEMIS instrument teams for providing the MS measurements required to complete this study. In addition, we would like to acknowledge the CCMC and BATS-R-US teams for providing the simulation results. The CCMC run numbers used in this paper are as follows: PS (Andrew_Dimmock_080714_1), SSW (Andrew_Dimmock_080714_4), FSW (Andrew_Dimmock_080714_3), NIMF (Andrew_Dimmock_080714_5) and SIMF (Andrew_Dimmock_080714_6).

Yuming Wang thanks the reviewers for their assistance in evaluating this paper.

References

Angelopoulos, V. (2008), The THEMIS mission, *Space Sci. Rev.*, *141*, 5–34, doi:10.1007/s11214-008-9336-1.

Balikhin, M. A., R. Z. Sagdeev, S. N. Walker, O. A. Pokhotelov, D. G. Sibeck, N. Beloff, and G. Dudnikova (2009), THEMIS observations of mirror structures: Magnetic holes and instability threshold, *Geophys. Res. Lett.*, *36*, L03105, doi:10.1029/2008GL036923.

Chen, Q., A. Otto, and L. C. Lee (1997), Tearing instability, Kelvin-Helmholtz instability, and magnetic reconnection, *J. Geophys. Res.*, *102*, 151–162, doi:10.1029/96JA03144.

Dimmock, A. P., and K. Nykyri (2013), The statistical mapping of magnetosheath plasma properties based on THEMIS measurements in the magnetosheath interplanetary medium reference frame, *J. Geophys. Res. Space Physics*, *118*, 4963–4976, doi:10.1002/jgra.50465.

Dimmock, A. P., K. Nykyri, and T. I. Pulkkinen (2014), A statistical study of magnetic field fluctuations in the dayside magnetosheath and their dependence on upstream solar wind conditions, *J. Geophys. Res. Space Physics*, *119*, 6231–6248, doi:10.1002/2014JA020009.

Dungey, J. W. (1961), Interplanetary magnetic field and the Auroral zones, *Phys. Rev. Lett.*, *6*, 47–48, doi:10.1103/PhysRevLett.6.47.

Fairfield, D. H. (1976), Magnetic fields of the magnetosheath, *Rev. Geophys.*, *14*, 117–134, doi:10.1029/RG014i001p00117.

Fairfield, D. H., and N. F. Ness (1970), Magnetic field fluctuations in the Earth's magnetosheath, *J. Geophys. Res.*, *75*(31), 6050–6060, doi:10.1029/JA075i031p06050.

Farris, M. H., and C. T. Russell (1994), Determining the standoff distance of the bow shock: Mach number dependence and use of models, *J. Geophys. Res.*, *99*(A9), 17,681–17,689, doi:10.1029/94JA01020.

Feldman, W. C., R. C. Anderson, S. J. Bame, S. P. Gary, J. T. Gosling, D. J. McComas, M. F. Thomsen, G. Paschmann, and M. M. Hoppe (1983), Electron velocity distributions near the Earth's bow shock, *J. Geophys. Res.*, *88*, 96–110, doi:10.1029/JA088iA01p00096.

Fujimoto, M., T. Terasawa, T. Mukai, Y. Saito, T. Yamamoto, and S. Kokubun (1998), Plasma entry from the flanks of the near-Earth magnetotail: Geotail observations, *J. Geophys. Res.*, *103*(A3), 4391–4408, doi:10.1029/97JA03340.

Génot, V., E. Budnik, P. Hellinger, T. Passot, G. Belmont, P. M. Trávníček, P.-L. Sulem, E. Lucek, and I. Dandouras (2009), Mirror structures above and below the linear instability threshold: Cluster observations, fluid model and hybrid simulations, *Ann. Geophys.*, *27*, 601–615, doi:10.5194/angeo-27-601-2009.

Hasegawa, H., M. Fujimoto, K. Maezawa, Y. Saito, and T. Mukai (2003), Geotail observations of the dayside outer boundary region: Interplanetary magnetic field control and dawn-dusk asymmetry, *J. Geophys. Res.*, *108*(A4), 1163, doi:10.1029/2002JA009667.

Hasegawa, H., M. Fujimoto, Y. Saito, and T. Mukai (2004), Dense and stagnant ions in the low-latitude boundary region under northward interplanetary magnetic field, *Geophys. Res. Lett.*, *31*, L06802, doi:10.1029/2003GL019120.

Hietala, H., N. Partamies, T. V. Laitinen, L. B. N. Clausen, G. Facskó, A. Vaivads, H. E. J. Koskinen, I. Dandouras, H. Rème, and E. A. Lucek (2012), Supermagnetosonic subsolar magnetosheath jets and their effects: From the solar wind to the ionospheric convection, *Ann. Geophys.*, *30*, 33–48, doi:10.5194/angeo-30-33-2012.

Hwang, K.-J., M. M. Kuznetsova, F. Sahraoui, M. L. Goldstein, E. Lee, and G. K. Parks (2011), Kelvin-Helmholtz waves under southward interplanetary magnetic field, *J. Geophys. Res.*, *116*, A08210, doi:10.1029/2011JA016596.

Janhunen, P. (1996), GUMICS-3 a global ionosphere-magnetosphere coupling simulation with high ionospheric resolution, in *Environment Modelling for Space-based Applications, Symposium Proceedings (ESA SP-392)*, edited by W. Burke and T.-D. Guyenne, p. 233, ESTEC, Noordwijk, Netherlands.

Janhunen, P., M. Palmroth, T. Laitinen, I. Honkonen, L. Juusola, G. Facskó, and T. I. Pulkkinen (2012), The GUMICS-4 global MHD magnetosphere-ionosphere coupling simulation, *J. Atmos. Sol. Terr. Phys.*, *80*, 48–59, doi:10.1016/j.jastp.2012.03.006.

Johnson, J. R., and C. Z. Cheng (2001), Stochastic ion heating at the magnetopause due to kinetic Alfven waves, *Geophys. Res. Lett.*, *28*, 4421–4424.

Johnson, J. R., C. Z. Cheng, and P. Song (2001), Signatures of mode conversion and kinetic Alfven waves at the magnetopause, *Geophys. Res. Lett.*, *28*, 227–230.

Karimabadi, H., H. X. Vu, D. Krauss-Varban, and Y. Omelchenko (2006), Global hybrid simulations of the Earth's magnetosphere, in *Numerical Modeling of Space Plasma Flows: Astronum-2006 ASP Conference Series*, vol. 359, edited by N. V. Pogorelov and G. P. Zank, Astron. Soc. of the Pacific, p. 257, San Francisco, Calif.

Karimabadi, H., B. Loring, H. X. Vu, Y. Omelchenko, M. Tatineni, A. Majumdar, U. Ayachit, and B. Geveci (2010), Numerical modeling of space plasma flows [electronic resource]: ASTRONUM-2010, paper presented at 5th International Conference of Numerical Modeling of Space Plasma Flows, San Diego, Calif., 13–18 June.

Karimabadi, H., B. Loring, P. O'Leary, A. Majumdar, M. Tatineni, and B. Geveci (2013), In-situ visualization for global hybrid simulations, in *Proceedings of the Conference on Extreme Science and Engineering Discovery Environment: Gateway to Discovery (XSEDE '13)*, Article 57, p. 8, ACM, New York, doi:10.1145/2484762.2484822.

Karimabadi, H., et al. (2014), The link between shocks, turbulence, and magnetic reconnection in collisionless plasmas, *Phys. Plasmas*, *21*(6), 62,308, doi:10.1063/1.4882875.

King, J. H., and N. E. Papitashvili (2005), Solar wind spatial scales in and comparisons of hourly Wind and ACE plasma and magnetic field data, *J. Geophys. Res.*, *110*, A02104, doi:10.1029/2004JA010649.

Kulsrud, R. (2005), *Plasma Physics for Astrophysics*, Princeton Univ. Press, N. J.

Lavraud, B., et al. (2013), Asymmetry of magnetosheath flows and magnetopause shape during low alfvén mach number solar wind, *J. Geophys. Res. Space Physics*, *118*, 1089–1100, doi:10.1002/jgra.50145.

Longmore, M., S. J. Schwartz, J. Geach, B. M. A. Cooling, I. Dandouras, E. A. Lucek, and A. N. Fazakerley (2005), Dawn-dusk asymmetries and sub-Alfvénic flow in the high and low latitude magnetosheath, *Ann. Geophys.*, *23*, 3351–3364, doi:10.5194/angeo-23-3351-2005.

Luhmann, J. G., C. T. Russell, and R. C. Elphic (1986), Spatial distributions of magnetic field fluctuations in the dayside magnetosheath, *J. Geophys. Res.*, *91*, 1711–1715, doi:10.1029/JA091iA02p01711.

McFadden, J. P., C. W. Carlson, D. Larson, M. Ludlam, R. Abiad, B. Elliott, P. Turin, M. Marckwordt, and V. Angelopoulos (2008), The THEMIS ESA plasma instrument and in-flight calibration, *Space Sci. Rev.*, *141*, 277–302, doi:10.1007/s11214-008-9440-2.

Nishino, M. N., M. Fujimoto, G. Ueno, T. Mukai, and Y. Saito (2007), Origin of temperature anisotropies in the cold plasma sheet: Geotail observations around the Kelvin-Helmholtz vortices, *Ann. Geophys.*, *25*, 2069–2086.

Němeček, Z., J. Šafránková, G. N. Zastenker, P. Pišoft, K. I. Paularena, and J. D. Richardson (2000), Observations of the radial magnetosheath profile and a comparison with gas dynamic model predictions, *Geophys. Res. Lett.*, *27*, 2801–2804, doi:10.1029/2000GL000063.

Němeček, Z., J. Šafránková, G. Zastenker, P. Pioft, and K. Jelínek (2002), Low-frequency variations of the ion flux in the magnetosheath, *Planet. Space Sci.*, *50*(5–6), 567–575, doi:10.1016/S0032-0633(02)00036-3.

Nykyri, K. (2013), Impact of MHD shock physics on magnetosheath asymmetry and Kelvin-Helmholtz instability, *J. Geophys. Res. Space Physics*, *118*, 5068–5081, doi:10.1002/jgra.50499.

Nykyri, K., and A. Otto (2001), Plasma transport at the magnetospheric boundary due to reconnection in Kelvin-Helmholtz vortices, *Geophys. Res. Lett.*, *28*(18), 3565–3568.
Nykyri, K., A. Otto, J. Büchner, B. Nikutowski, W. Baumjohann, L. M. Kistler, and C. Mouikis (2003), Equator-S observations of boundary signatures: FTE's or Kelvin-Helmholtz waves?, in *Earth's Low-Latitude Boundary Layer*, edited by P. T. Newell and T. Onsager, pp. 205–210, AGU, Washington, D. C.
Nykyri, K., A. Otto, B. Lavraud, C. Mouikis, L. M. Kistler, A. Balogh, and H. Rème (2006), Cluster observations of reconnection due to the Kelvin-Helmholtz instability at the dawnside magnetospheric flank, *Ann. Geophys.*, *24*, 2619–2643, doi:10.5194/angeo-24-2619-2006.
Otto, A., and D. H. Fairfield (2000), Kelvin-Helmholtz instability at the magnetotail boundary: MHD simulation and comparison with Geotail observations, *J. Geophys. Res.*, *105*(A9), 21,175–21,190.
Palmroth, M., P. Janhunen, T. I. Pulkkinen, A. Aksnes, G. Lu, N. Østgaard, J. Watermann, G. D. Reeves, and G. A. Germany (2005), Assessment of ionospheric Joule heating by GUMICS-4 MHD simulation, AMIE, and satellite-based statistics: Towards a synthesis, *Ann. Geophys.*, *23*, 2051–2068, doi:10.5194/angeo-23-2051-2005.
Papadopoulos, K. (1985), Microinstabilities and anomalous transport, in *Collisionless Shocks in the Heliosphere: A Tutorial Review*, vol. 34, edited by R. G. Stone and B. T. Tsurutani, pp. 59–90, AGU, Washington, D. C.
Paularena, K. I., J. D. Richardson, M. A. Kolpak, C. R. Jackson, and G. L. Siscoe (2001), A dawn-dusk density asymmetry in Earth's magnetosheath, *J. Geophys. Res.*, *106*, 25,377–25,394, doi:10.1029/2000JA000177.
Petrinec, S. M., T. Mukai, A. Nishida, T. Yamamoto, T. K. Nakamura, and S. Kokubun (1997), Geotail observations of magnetosheath flow near the magnetopause, using Wind as a solar wind monitor, *J. Geophys. Res.*, *102*, 26,943–26,960, doi:10.1029/97JA01637.
Russell, C. T., and R. C. Elphic (1979), ISEE observations of flux transfer events at the dayside magnetopause, *Geophys. Res. Lett.*, *6*, 33–36, doi:10.1029/GL006i001p00033.
Sagdeev, R. Z. (1966), Cooperative phenomena and shock waves in collisionless plasmas, *Rev. Plasma Phys.*, *4*, 23–90.
Sagdeev, R. Z., and A. A. Galeev (1969), *Nonlinear Plasma Theory*, Benjamin, New York.
Shevyrev, N., and G. Zastenker (2005), Some features of the plasma flow in the magnetosheath behind quasi-parallel and quasi-perpendicular bow shocks, *Planet. Space Sci.*, *53*(1–3), 95–102, doi:10.1016/j.pss.2004.09.033.
Shevyrev, N., G. Zastenker, P. Eiges, and J. Richardson (2006), Low frequency waves observed by Interball-1 in foreshock and magnetosheath, *Adv. Space Res.*, *37*(8), 1516–1521, doi:10.1016/j.asr.2005.07.072.
Shevyrev, N. N., G. N. Zastenker, and J. Du (2007), Statistics of low-frequency variations in solar wind, foreshock and magnetosheath: Interball-1 and Cluster data, *Planet. Space Sci.*, *55*, 2330–2335, doi:10.1016/j.pss.2007.05.014.
Shue, J.-H., et al. (1998), Magnetopause location under extreme solar wind conditions, *J. Geoplys. Res.*, *103*, 17,691–17,700, doi:10.1029/98JA01103.
Sibeck, D. G. (1990), A model for the transient magnetospheric response to sudden solar wind dynamic pressure variations, *J. Geophys. Res.*, *94*(A4), 3755–3771.
Sibeck, D. G. (1992), Transient events in the outer magnetosphere: Boundary waves or FTEs?, *J. Geophys. Res.*, *97*, 4009–4026.
Sibeck, D. G., and M. F. Smith (1992), Magnetospheric plasma flows associated with, boundary waves and flux transfer events, *Geophys. Res. Lett.*, *19*, 1903–1906.
Soucek, J., and C. P. Escoubet (2011), Cluster observations of trapped ions interacting with magnetosheath mirror modes, *Ann. Geophys.*, *29*, 1049–1060, doi:10.5194/angeo-29-1049-2011.
Soucek, J., E. Lucek, and I. Dandouras (2008), Properties of magnetosheath mirror modes observed by Cluster and their response to changes in plasma parameters, *J. Geophys. Res.*, *113*, A04203, doi:10.1029/2007JA012649.
Spreiter, J. R., A. L. Summers, and A. Y. Alksne (1966), Hydromagnetic flow around the magnetosphere, *Planet. Space Sci.*, *14*, 223–250, doi:10.1016/0032-0633(66)90124-3.
Tóth, G., et al. (2005), Space weather modeling framework: A new tool for the space science community, *J. Geophys. Res.*, *110*, A12226, doi:10.1029/2005JA011126.
Verigin, M. I., et al. (2001), Analysis of the 3-D shape of the terrestrial bow shock by Interball/Magion 4 observations, *Adv. Space Res.*, *28*, 857–862, doi:10.1016/S0273-1177(01)00502-6.
Verigin, M. I., M. Tátrallyay, G. Erdős, and G. A. Kotova (2006), Magnetosheath interplanetary medium reference frame: Application for a statistical study of mirror type waves in the terrestrial plasma environment, *Adv. Space Res.*, *37*, 515–521, doi:10.1016/j.asr.2005.03.042.
Walsh, B. M., D. G. Sibeck, Y. Wang, and D. H. Fairfield (2012), Dawn-dusk asymmetries in the Earth's magnetosheath, *J. Geophys. Res.*, *117*, A12211, doi:10.1029/2012JA018240.
Wang, C.-P., M. Gkioulidou, L. R. Lyons, and V. Angelopoulos (2012), Spatial distributions of the ion to electron temperature ratio in the magnetosheath and plasma sheet, *J. Geophys. Res.*, *117*, A08215, doi:10.1029/2012JA017658.
Wing, S., and P. T. Newell (1998), Central plasma sheet ion properties as inferred from ionospheric observations, *J. Geophys. Res.*, *103*, 6785–6800, doi:10.1029/97JA02994.
Wing, S., J. R. Johnson, P. T. Newell, and C.-I. Meng (2005), Dawn-dusk asymmetries, ion spectra, and sources in the northward interplanetary magnetic field plasma sheet, *J. Geophys. Res.*, *110*, A08205, doi:10.1029/2005JA011086.
Yao, Y., C. C. Chaston, K.-H. Glassmeier, and V. Angelopoulos (2011), Electromagnetic waves on ion gyro-radii scales across the magnetopause, *Geophys. Res. Lett.*, *38*, L09102, doi:10.1029/2011GL047328.
Zastenker, G., M. Nozdrachev, Z. Němeček, J. Šafránková, K. Paularena, J. Richardson, R. Lepping, and T. Mukai (2002), Multispacecraft measurements of plasma and magnetic field variations in the magnetosheath: Comparison with spreiter models and motion of the structures, *Planet. Space Sci.*, *50*(5–6), 601–612, doi:10.1016/S0032-0633(02)00039-9.